Modeling evidence for enhanced El Niño–Southern Oscillation amplitude during the Last Glacial Maximum

S.-I. An,[1] A. Timmermann,[2,3] L. Bejarano,[4] F.-F. Jin,[4] F. Justino,[2,5] Z. Liu,[6] and A. W. Tudhope[7]

[1] We present a numerical eigenmode analysis of an intermediate El Niño–Southern Oscillation (ENSO) model which is driven by present-day observed background conditions as well as by simulated background conditions for the Last Glacial Maximum (LGM) about 21,000 years ago. The background conditions are obtained from two LGM simulations which were performed with the National Center for Atmospheric Research climate system model (CSM1.4) and an Earth system model of intermediate complexity (ECBilt-CLIO). Our analysis clearly shows that the leading present-day unstable recharge-discharge mode changes its stability as well as its frequency during LGM conditions. Simulated LGM background conditions were favorable to support large-amplitude self-sustained interannual ENSO variations in the tropical Pacific. Our analysis indicates that off-equatorial climate conditions as well as a shoaling of the thermocline play a crucial role in amplifying the LGM ENSO mode. *INDEX TERMS:* 1615 Global Change: Biogeochemical processes (4805); 3344 Meteorology and Atmospheric Dynamics: Paleoclimatology; 4215 Oceanography: General: Climate and interannual variability (3309); 4271 Oceanography: General: Physical and chemical properties of seawater; 4522 Oceanography: Physical: El Nino; *KEYWORDS:* ENSO, Last Glacial Maximum, eigenmode

1. Introduction

[2] The El Niño–Southern Oscillation (ENSO) is a coupled tropical mode of interannual climate variability which involves oceanic dynamics [*Jin*, 1997] as well as large-scale atmospheric changes [*Bjerknes*, 1969; *Gill*, 1982]. Through anomalous diabatic heating El Niño and La Niña conditions trigger meridionally propagating atmospheric Rossby waves which encompass weather conditions even in high latitudes. Recent greenhouse warming simulations performed with ENSO-resolving coupled general circulation models (CGCMs) have revealed a high degree of uncertainty with respect to the amplitude and the pattern of future tropical Pacific warming [e.g., *Timmermann et al.*, 1999; *Collins*, 2000]. Furthermore, the response of ENSO to an anticipated anthropogenic warming appears to be highly model-dependent. In the work of *Timmermann* [2001] it was suggested that the ENSO response to greenhouse warming not only depends on the mean warming pattern but also on how far away in parameter space the model ENSO operates from supercriticality. An independent way to calibrate CGCMs is to study their behavior under extreme paleo conditions. Here we choose the Last Glacial Maximum (LGM) which was characterized by reduced CO_2 conditions, Northern Hemispheric ice caps, different vegetation and lowered sea level. LGM paleotemperature reconstructions for the tropical Pacific are ambivalent. While some studies [*Lea et al.*, 2000] show a strong cold tongue cooling of about 4 degrees which outweighs the warm pool cooling of about 2.8 ± 0.8 K, others [*Koutavas et al.*, 2002] are more consistent with an El Niño-type pattern. Past ENSO variability has been reconstructed for small time slices throughout the last 120,000 years [*Sandweiss et al.*, 1996; *Hughen et al.*, 1999; *Rodbell et al.*, 1999; *Rittenour et al.*, 2000; *Corrège et al.*, 2000; *Tudhope et al.*, 2001; *Moy et al.*, 2002; *Andrus et al.*, 2002; *Cobb et al.*, 2003; *Woodroffe et al.*, 2003]. The coral data of *Hughen et al.* [1999] suggest that ENSO was active during the last interglacial about 125,000 years ago and was probably reduced in its activity [*Rodbell et al.*, 1999; *Moy et al.*, 2002; *Tudhope et al.*, 2001] during the early to mid-Holocene (9000–6000 years ago). Figure 1 shows the power spectrum of $\delta^{18}O$ variations from a present-day and three fossil corals sampled at Papua New-Guinea. These isotope variations capture mostly interannual rainfall variability associated with ENSO. For the three fossil corals from the last glacial period (corals are about 38–42 kyr old) one observes a reduction of the interannual

[1]International Pacific Research Center, University of Hawaii, Honolulu, Hawaii, USA.

[2]Leibniz Institut für Meereswissenschaften, IfM-GEOMAR, Kiel, Germany.

[3]Now at International Pacific Research Center, University of Hawaii, Honolulu, Hawaii, USA.

[4]Department of Meteorology, Florida State University, Tallahassee, Florida, USA.

[5]Now at Department of Physics, University of Toronto, Toronto, Ontario, Canada.

[6]Center for Climatic Research, University of Wisconsin-Madison, Madison, Wisconsin, USA.

[7]School of Geosciences, Edinburgh University, Edinburgh, UK.
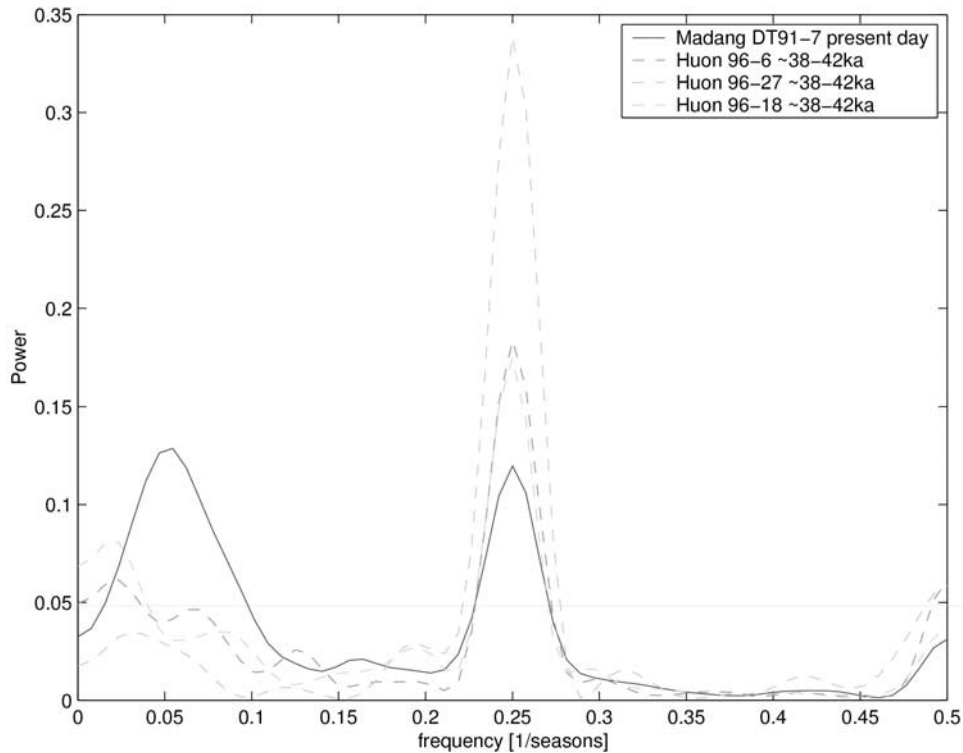
Figure 1. Power spectra of $\delta^{18}O$ time series obtained from an isotope analysis of fossil (dashed) and modern (solid) corals sampled in Papua New Guinea. Data from *Tudhope et al.* [2001]. See color version of this figure at back of this issue.

ENSO variance (2–8 year periodicity band) relative to the modern. Here we disregard potential changes of the main periodicities during the last glacial period, which are difficult to assess due to the limited sampling length of the fossil corals. The apparent difference in the strength of the seasonal cycle in the coral isotope records between modern and glacial in Figure 1 is due mainly to the different sampling locations. i.e., in modern coral isotope records, although the amplitude of interannual ENSO variance is similar between Madang and the Huon [e.g., *Tudhope et al.*, 2001, Figure 3], the amplitude of the seasonal cycle is smaller at Madang. Comparison of short (18-year- long) modern coral records from Huon with the glacial corals from the same site (not shown) indicates that the amplitude of the seasonal cycle at this site was similar during both periods.

[3] Under the assumption that the ENSO teleconnection pattern remains stable, this would suggest that glacial ENSO variability was smaller than today's. However, this fundamental assumption might not be valid as argued by *Otto-Bliesner et al.* [2003].

[4] A whole series of global coupled atmosphere-ocean simulations has been performed to study certain aspects of the LGM climate [e.g., *Bush and Philander*, 1998; *Shin et al.*, 2003; *Liu et al.*, 2002; *Kitoh et al.*, 2001; *Hewitt et al.*, 2001; *Timmermann et al.*, 2004; *Kim et al.*, 2003; *Peltier and Solheim*, 2004]. The overall simulated sea surface temperature (SST) response to glacial boundary conditions is highly model-dependent. Still most authors claim that their simulated SST patterns are in agreement with some of

the paleo SST reconstructions. Despite significant uncertainties in both the models and the paleodata interpretation, it is informative to study the sensitivity of ENSO to glacial boundary conditions, as done by *Otto-Bliesner et al.* [2003] and *Peltier and Solheim* [2004]. These two descriptive studies, using a similar version of the NCAR CSM1.4 climate model suggest an amplification of ENSO variance during the LGM, which has been attributed to changes of the oceanic stratification [*Otto-Bliesner et al.*, 2003].

[5] Here we address this issue by performing an eigenanalysis of an intermediate tropical coupled atmosphere-ocean model which is driven by present-day climate background conditions and perturbed background conditions which capture the anomalies between LGM and present-day climate.

[6] The LGM background changes are obtained from two different LGM simulations performed with the state-of-the-art coupled general circulation model NCAR CSM, Version 1.4 [*Otto-Bliesner et al.*, 2003] and Earth system model of intermediate complexity ECBilt-CLIO, version 3.0 [*Goosse et al.*, 2002; *Timmermann et al.*, 2004]. The LGM experiments use glacial boundary conditions such as the LGM continental ice sheet extension, reduced levels in the atmospheric trace gases, and Milankovitch solar radiation changes [*Shin et al.*, 2003]. In addition the NCAR CSM1.4 model also captures a lowering of global sea level of about 120 m. The CSM1.4 LGM simulation shows an enhancement of ENSO variability as compared to the present-day control simulation which has been attributed [*Otto-Bliesner et al.*, 2003] to changes of the zonal SST

gradient, wind stress, upwelling and in particular a sharpening of the thermocline. In contrast, the low-resolution model ECBilt-CLIO does not simulate ENSO dynamics and will be used here only to study the stability of the simulated glacial background state.

[7] Our paper is organized as follows: in section 2 we describe the technique used to study ENSO variability during the LGM. In section 3 we present the eigenanalysis based on the LGM background conditions simulated by the CSM model. Our paper concludes with a discussion and summary of our main results.

2. Eigenmode Analysis of an Intermediate ENSO Model

[8] In order to systematically understand how LGM background changes, as simulated by *Shin et al.* [2003], *Otto-Bliesner et al.* [2003] and *Timmermann et al.* [2004], affect ENSO variability we perform an eigenanalysis of a more simplified dynamical model using different background states. Our model is similar to the intermediate ENSO model of *Zebiak and Cane* [1987]. Our model differs from the original [*Zebiak and Cane*, 1987] model in employing smoothed versions of the subsurface temperature parameterization, vertical advection and the convergence feedback. Furthermore, an improved advection scheme has been used which treats the horizontal advection of temperature anomalies properly. Furthermore, the atmospheric model is solved explicitly, rather than iteratively. This leads to regular ENSO oscillations with a small skewness, in contrast to the highly chaotic and strongly skewed oscillations of the *Zebiak and Cane* [1987] model. Overall, the period of the ENSO oscillation in both models is similar.

[9] In order to reduce the matrix dimension of the linear dynamical operator the ocean dynamic fields have been expanded spectrally using Hermite functions, as in the work of *Battisti* [1988]. For different climate background conditions we compute the Jacobian matrix using a perturbation method in which the matrix elements are computed from small variable perturbations and their simulated corresponding time derivatives. As will be shown in a forthcoming paper this method is very robust and approximates the Jacobian matrix quite well. In our case the size of the Jacobian matrix is 1439×1439. Eventually, the eigenmodes are computed using standard numerical eigenanalysis techniques. However, in many fluid-dynamical systems the estimation of eigenmodes can be difficult, because small errors in the matrix estimation may give rise to large errors of the eigenvalues, due to the nonnormality of the linear operators. This effect can be quantified by using pseudospectral methods [*Trefethen*, 1999] which provide uncertainty bounds for the linear eigenmodes. In order to show that our eigenmode solutions are robust we have also computed the pseudospectra [*Trefethen*, 1999] of the Jacobian matrix. The results (not shown here) indicate that small errors in the computation of the matrix elements of a few percent do not modify the eigenspectrum of the leading modes significantly, despite the nonnormality of the tropical coupled atmosphere-ocean system. Instead of using the full CSM and ECBilt-CLIO

background control and LGM states for the eigenanalysis of the *Zebiak and Cane* [1987]-type model we use the observed background state $\vec{X}_{ZC}$ which consists of the mean SST, thermocline depth, surface winds, wind divergence, horizontal and vertical current fields and perturb these fields by the diagnosed difference between the LGM and present-day (CTR) simulation. We obtain the background state (BG) from $\vec{X}_{BG} = \vec{X}_{ZC} + \gamma(\vec{X}_{LGM} - \vec{X}_{CTR})$, where γ can vary between zero and one. A γ value of 0 represents present-day conditions, and a γ value of 1 corresponds to LGM conditions.

## 3. Eigenmode Analysis of Present-Day and LGM ENSO

3.1. CSM1.4 Results

[10] Figure 2 shows the simulated changes of the SST, the surface winds, the horizontal currents in the surface layer, upwelling, and the thermocline depth between the CSM LGM simulation and the present-day control run. Our intermediate model does not include continental topography, such that land anomalies from the CSM simulation are interpolated to the oceanic grid of the intermediate ENSO model. As discussed by *Shin et al.* [2003] one observes a cooling of the warm pool area and a less strong cooling of the cold tongue. Furthermore, a mean shoaling of the thermocline can be observed which can be attributed to an inflow of cold Southern Pacific thermocline waters [*Liu et al.*, 2002]. The difference between the LGM and present-day CSM experiment, as shown in Figure 2 is added, as a perturbation to the observed mean state of our intermediate ENSO model. Eventually a new Jacobian matrix is computed for this new background state and the eigenmodes of this matrix are computed.

[11] Figure 3 (right panel) shows the eigenmodes of the observed background state. In addition to the so-called damped scatter modes, one observes an unstable mode with a period of 3.8 years. This mode corresponds to the leading recharge-discharge ENSO mode of the system. The scatter modes are free planetary wave modes which satisfy the given boundary condition of no net mass flow along the western boundary and the long-wave approximation for a given spectral truncation [*Liu*, 2002]. They will not be considered here in detail. The eigenmode spectrum for the LGM perturbation conditions also exhibits an unstable interannual mode with a period of about 3.7 years. The LGM ENSO mode is more unstable than the present-day ENSO mode. The enhanced growth rate during the LGM is consistent with an increased ENSO amplitude [*Otto-Bliesner et al.*, 2003] in the LGM-CGCM simulation. If ENSO operates in a self-sustained regime not too far away from the initial Hopf bifurcation point, as in our case, growth rate and amplitude are related to each other by a monotonous nonlinear function. Hence the growth rate can be used as a measure of amplitude. The advantage of our systematic analysis is that we can disentangle which component of the background changes is most important for the LGM ENSO behavior. We performed an eigenanalysis which is based on the LGM perturbation only in the equatorial region. The background state $\vec{x}_{BG}$ was modified using a Gaussian latitudinal weighting function
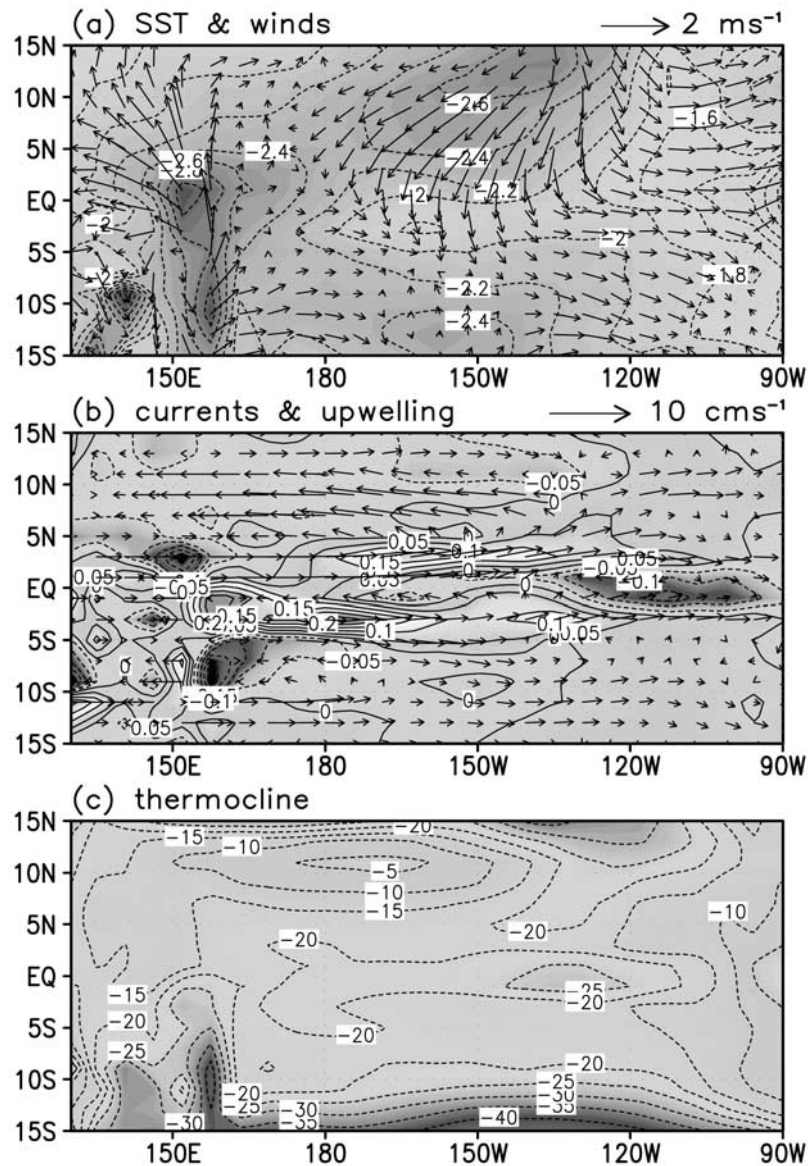
Figure 2. Simulated difference of SST (K), wind (m/s), surface current (cm/s), upwelling (10^{-3} cm/s) and thermocline depth (m) between CSM LGM and present-day simulation. Data are interpolated onto the grid of our intermediate tropical model. See color version of this figure at back of this issue.
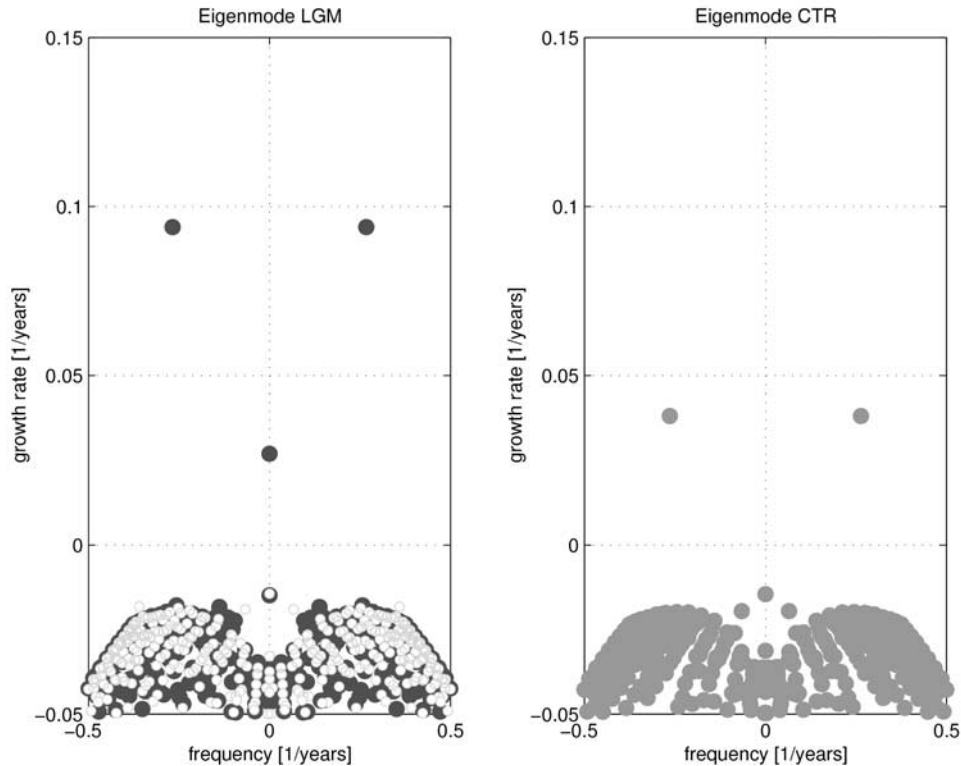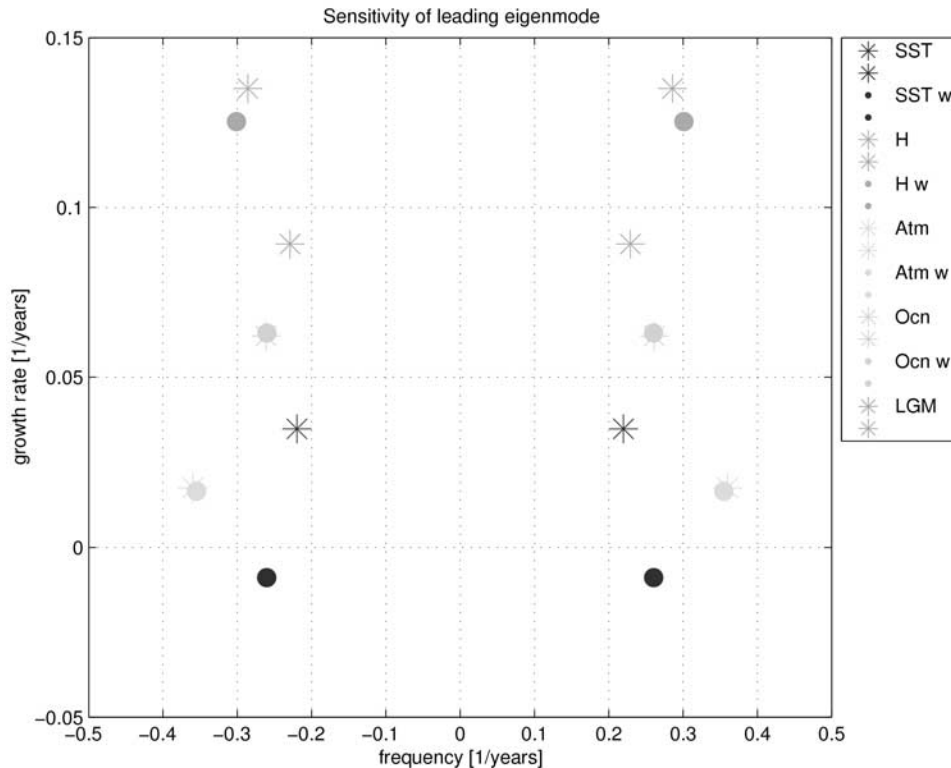
Figure 3. Eigenmodes of the linearized ZC-type intermediate ENSO model for (left) glacial and (right) present-day background conditions as simulated by the CSM1.4 model. The light blue dots represent the leading eigenmode using LGM background conditions if extratropical anomalies are neglected. The eigenspectrum is symmetric around the zero frequency. See color version of this figure at back of this issue.

with a width of about 10 degrees. The latitudinal weighting effectively leaves the equatorial anomalies intact, while damping the off-equatorial anomalies strongly, depending on the width of the Gaussian weighting function. We have not tested the sensitivity of our results with respect to the width of the Gaussian weighting function. The new eigenvalue spectrum (Figure 3, left panel, light blue dot) exhibits a damped ENSO mode with an eigenfrequency of 0.3 1/years and a negative growth rate of -0.02 1/year which is almost indistinguishable from the scatter spectrum. This damped ENSO mode can be identified (not shown) by the pattern evolution of the eigenvectors, which is consistent with a damped mixed-SST wave mode. ENSO can still exist as a physical mode (solution) of the system, even when its growth rate is negative. In order to appear in a forward simulation, however, noise or other kind of external perturbations are needed. From Figure 3 we conclude that the off-equatorial regions play an important role in amplifying ENSO variability during the LGM.

[12] This is further illustrated in Figure 4 showing the sensitivity of the leading eigenmode to background condition changes in only one variable and to latitudinal weighting. In comparison with the growth rate of the present-day leading ENSO eigenmode (see Figure 3, right panel) we see that LGM changes in the oceanic currents (yellow star and circle) do not influence the growth rate of the leading eigenmode significantly, in contrast to the effect of the LGM thermocline anomaly field (light blue star and circle)

which leads to an intensification of ENSO variability, and the atmospheric field (green star and circle) which damps ENSO variability. If the prevailing winds are strong enough a shallower mean thermocline as observed in Figure 2 may lead to an intensification of ENSO variability as discussed in the work of *Fedorov and Philander* [2000]. In Figure 2 we observe a weakening of the equatorial trades in the tropical eastern Pacific which may also lead to a reduction of ENSO variability. Furthermore, we see a large difference between the eigenmodes of the total LGM SST field (red circle) and the latitudinally weighted field (red star). In the former case we observe a growth rate of 0.03 1/year, in the latter the ENSO mode is damped. Hence in addition to the overall equatorial thermocline shoaling, off-equatorial SST changes seem to be important in amplifying ENSO during the LGM. This can be explained by the meridional advection term $-v'\partial\overline{T}/\partial y$ which has a smaller magnitude during the LGM. Under present-day conditions (due to the presence of the equatorial cold tongue) the meridional temperature gradient is positive north of the equator. Under LGM conditions the northern off-equatorial regions cool more than the equator (see Figure 2), which leads to a weakening of the meridional temperature gradient Since the anomalous meridional advection of the mean temperature gradient provides a negative heating for present-day ENSO conditions [*Kang et al.*, 2001] a weakened meridional temperature gradient leads to a weaker negative feedback and hence to an intensification of ENSO variability during

Figure 4. Sensitivity of the leading eigenmodes of the linearized ZC-type intermediate ENSO model with respect to latitudinal weighting (w) and LGM changes in only one variable of the climate background conditions. SST indicates LGM changes are taken into account only for the SST background field. Abbreviations are as follows: H, thermocline depth changes; Atm., wind and wind-divergence changes; Ocn., changes of the oceanic currents; LGM, changes of all background fields. See color version of this figure at back of this issue.

the LGM. In conclusion, we can say that both the mean thermocline shoaling (light blue) during the LGM as well as changes of the mean meridional temperature gradient lead to a significant intensification of LGM ENSO variability.

[13] The physical mechanism of ENSO under present-day and LGM conditions can be elucidated further by studying the spatiotemporal evolution of SST and thermocline anomalies. Figure 5 displays the time evolution of the present-day (upper panels) and LGM (lower panels) leading ENSO eigenmode in equatorial SST, thermocline and zonal current anomalies. As compared to the present-day eigenmode of the linearized intermediate model, the LGM mode exhibits a slight tendency toward eastward propagating SST anomalies. As shown by *Jin et al.* [2003] eastward propagating El Niño events are typically characterized by larger amplitudes due to nonlinear dynamic heating. The thermocline field is in accordance with the recharge-mechanism for ENSO [*Jin*, 1997]. Furthermore, we observe that both during present-day and LGM conditions the warm pool temperature advection plays an important role in amplifying the temperature anomalies in the central Pacific during El Niño and La Niña conditions.

3.2. ECBilt-CLIO Results

[14] We have also performed an eigenanalysis of the LGM background state as simulated by the ECBilt-CLIO model

[*Timmermann et al.*, 2004]. This global coupled atmosphere-ocean-sea-ice model underestimates tropical variability due to the low atmospheric resolution and the quasigeostrophic approximation used in the atmospheric model. The LGM simulation represents an extreme case for tropical climate change during the LGM. The ECBilt-CLIO model simulates a La Niña-type pattern for the LGM with enhanced trade winds and ocean currents, as shown in Figure 6. The corresponding eigenanalysis exhibits an unstable oscillatory LGM-ENSO mode as shown by Figure 7. We have changed the parameter γ which controls the ratio between LGM and CTR background conditions. Figure 7 clearly reveals that the unstable fast LGM mode becomes more and more stable, as we go from LGM to control conditions.

[15] The ECBilt-CLIO background changes suggest enhanced interannual ENSO variability during the LGM. Despite the differences in the simulated background conditions in the CSM1.4 and ECBilt-CLIo model, both LGM simulations are consistent with an intensification of ENSO variability.

4. Summary and Conclusions

[16] We have presented modeling evidence that the LGM background conditions in the tropical Pacific as simulated by the CSM1.4 and the ECBilt-CLIO model are favorable
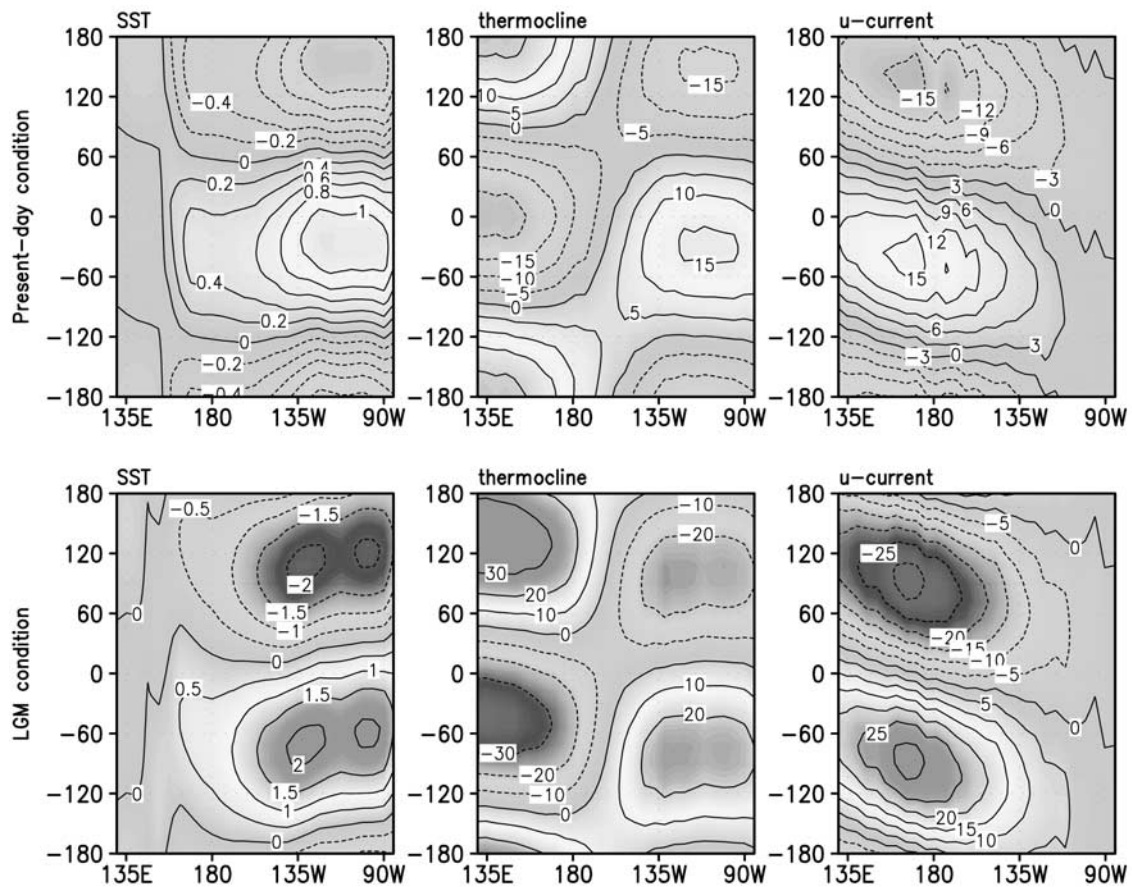
Figure 5. Hovmoller diagram of the leading eigenvector of the linearized ZC-type intermediate ENSO model for observed (upper panels) present-day and (lower panels) glacial background conditions simulated by the CSM model. Only the SST, thermocline depth, and current anomalies are displayed. The time evolution represented by the phase on the y axes is directed upward. See color version of this figure at back of this issue.
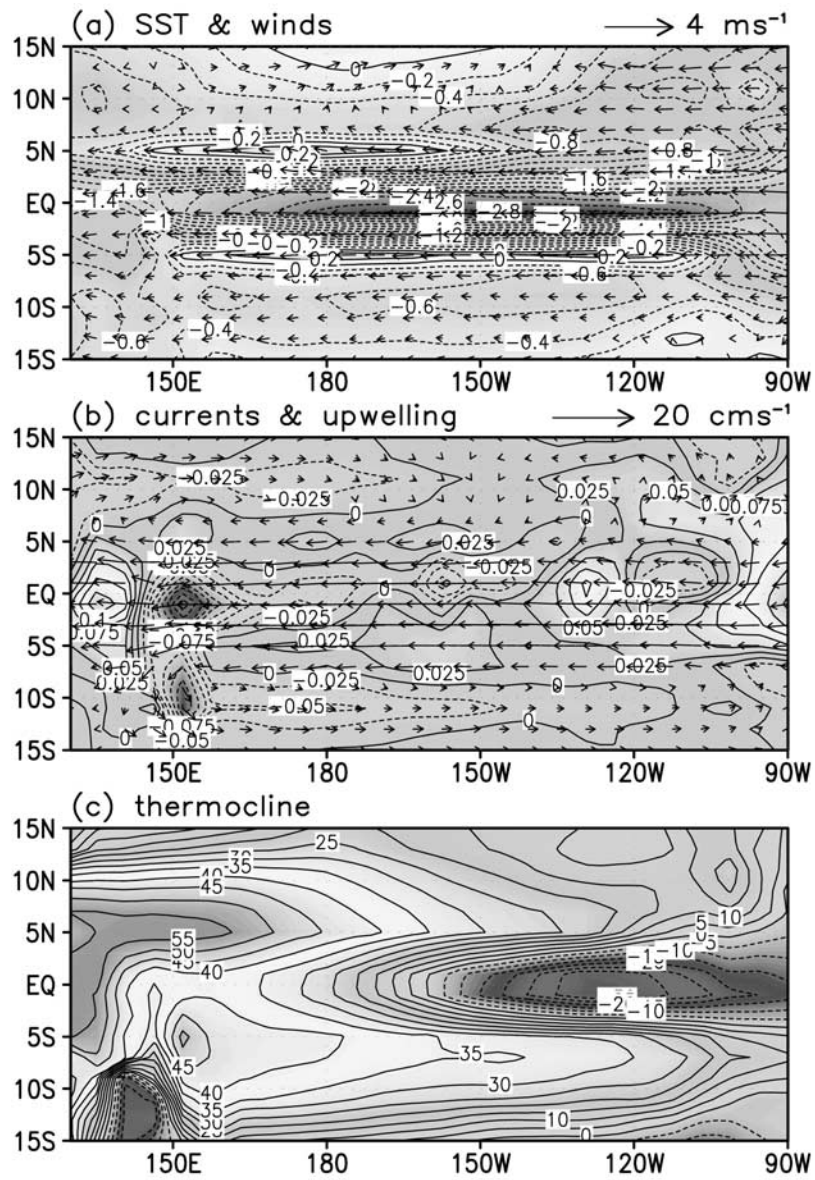
Figure 6. Simulated difference of SST (K), wind (m/s), surface current (cm/s), upwelling (10^{-3}cm/s) and thermocline depth (m) between ECBilt-CLIO LGM and present-day simulation. Data are interpolated onto the grid of our intermediate tropical model. See color version of this figure at back of this issue.
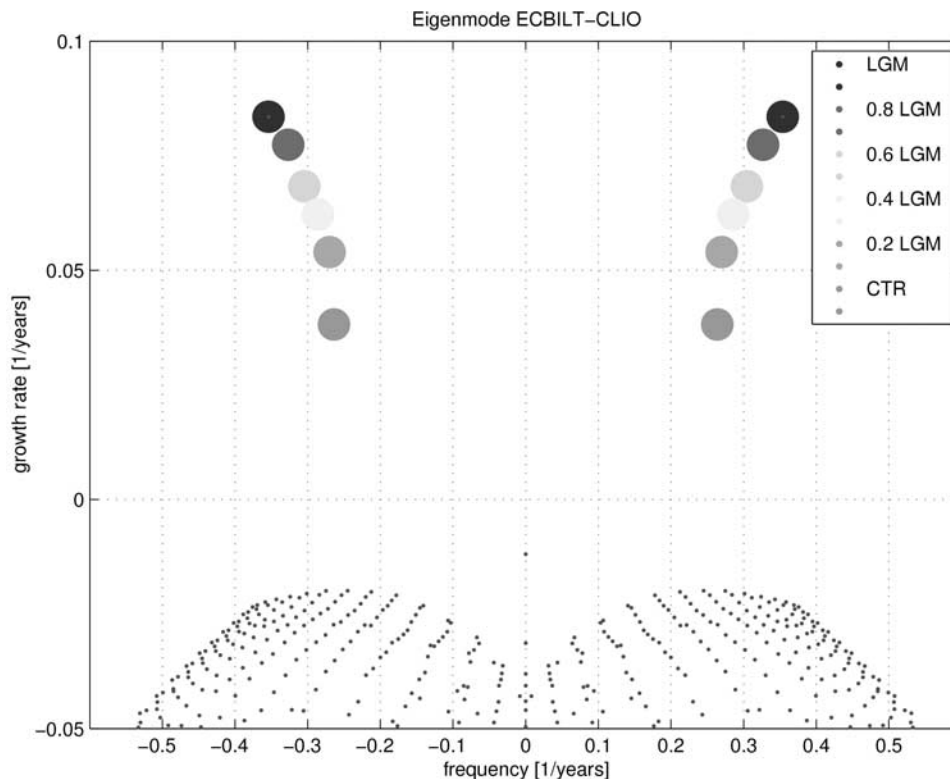
Figure 7. Eigenmode spectrum (dark blue) for the LGM background perturbation simulated by the ECBilt-CLIO model. Colored dots: Leading eigenmodes for different values of γ as defined by $\vec{X}_{BG} = \vec{X}_{ZC} + \gamma(\vec{X}_{LGM} - \vec{X}_{CTR})$. Red dot: leading eigenmode of the intermediate ENSO model forced by present-day climate background conditions. See color version of this figure at back of this issue.

for the generation of interannual recharge-discharge ENSO variations, thereby confirming the main conclusion of *Otto-Bliesner et al.* [2003] and *Peltier and Solheim* [2004]. In contrast to the diagnostic study of *Otto-Bliesner et al.* [2003] however, we find that it is mostly a shoaling of the thermocline which leads to stronger ENSO variability in the CSM1.4 LGM simulation, rather than a sharpening. In fact an analysis (not shown) of the simulated equatorial temperature structure shows no clear sign for a sharpening of the equatorial thermocline. However, further sensitivity tests with the intermediate ENSO model have revealed that in general changes of the thermocline sharpness may have a strong effect on ENSO growth rate.

[17] While the LGM ENSO variance in the CSM1.4 model is amplified due to a combination of thermocline and meridional temperature gradient changes, the ECBilt-Clio LGM ENSO amplification is consistent with the two-parameter ENSO regime diagram (wind and mean thermocline depth) of *Fedorov and Philander* [2000]: An amplification of the trade winds leads to an amplification of ENSO variance as well as to shorter periodicities (see Figures 6, 7).

[18] Our mathematical analysis also has several disadvantages: Our eigenanalysis does not provide a direct quantification of the amplitude of ENSO. We have used ENSO amplitude and growth rate synonymously. In fact the amplitude of ENSO in a limit cycle regime is determined by the nonlinearities which cannot be assessed directly by our linear eigenanalysis. Hence we have also performed numerical simulations using our intermediate model forced by differences between the present-day and LGM background states These simulations (not shown) support the main conclusion of the eigenanalysis.

[19] Another caveat of our modeling approach is that we prescribe an annual mean state, as in the work of *Fedorov and Philander* [2000], neglecting the annual cycle forcing. Annual cycle forcing may be a very important process controlling the strength of ENSO variability. A Floquet analysis taking into account a seasonally varying background state might be appropriate but would exceed the scope of our paper.

[20] Intensified ENSO variability, as found in our analysis and supported by *Otto-Bliesner et al.* [2003] is not necessarily inconsistent with coral data of [*Tudhope et al.*, 2001]. In fact, as shown by *Otto-Bliesner et al.* [2003] weakened ENSO teleconnection patterns may also lead to a reduction of interannual rainfall variability in the warm pool area. There exists a large uncertainty in the simulated LGM temperature anomaly patterns in the tropical oceans. For instance, *Bush and Philander* [1998] simulate a cooling of the tropical oceans of about 4–6 degrees in their LGM simulation, whereas the tropical cooling in the *Kim et al.* [2003] simulation attains values of up to 8 degrees. On the other hand *Shin et al.* [2003], *Hewitt et al.* [2001], *Timmermann et al.* [2004] and *Kitoh et al.* [2001] find a

more moderate cooling of about 2–3 degrees. These large discrepancies are not too surprising, given the uncertainty of future climate projections using state-of-the-art coupled general circulation models. Surprising however is that all of these LGM model simulations are considered to be consistent with reconstructed data. Obviously this suggests that the uncertainty in the reconstructions also is large and not yet sufficient to constrain which of the model simulations is most realistic.

[21] The uncertainty in the LGM background states (Figures 2 and 6) also raises the question as to what has controlled the temperatures in the tropical Pacific during the LGM. Two different hypothesis have been suggested to explain the equatorial cooling of 2–5 K in the Pacific. *Liu et al.* [2002] argue based on the CSM coupled model simulation that the subduction of anomalously cold water from the Southern Hemisphere leads to a shoaling of the equatorial thermocline. Using the ECBilt-Clio LGM simulation *Timmermann et al.* [2004] argue, on the other hand that changes in the transient and stationary wave activity in the North Pacific lead to a remote intensification of the trade winds, which in turn lead to an enhancement of equatorial upwelling by spinning up the subtropical cells. In addition, in both simulations, reduced water vapor and CO_2 concentrations generate a local cooling in the tropical areas. Our study should be regarded as a first step toward an assessment of ENSO's response to glacial boundary conditions.

[22] In addition, further paleoproxy data have to be collected and processed in order to quantify the response of ENSO to LGM boundary conditions. Comparing LGM simulations of ENSO with new reconstructed data might also help to assess the validity of future greenhouse projections. The LGM can be used as an independent calibration period for CGCM simulations.

References

Andrus, C. F., D. E. Crowe, D. H. Sandweiss, E. J. Reitz, and C. S. Romanek (2002), Otolith $\delta^{18}O$ records of mid-Holocene sea surface temperatures in Peru, *Science*, *295*, 1508–1510.

Battisti, D. (1988), The dynamics and thermodynamics of a warming event in a coupled tropical ocean/atmosphere model, *J. Atmos. Sci.*, *45*, 2889–2919.

Bjerknes, J. (1969), Atmospheric teleconnections from the equatorial Pacific, *Mon. Weather Rev.*, *97*, 163–172.

Bush, A. B. G., and S. G. H. Philander (1998), The role of ocean-atmosphere interactions in tropical cooling during the Last Glacial Maximum, *Science*, *279*, 1341–1344.

Cobb, K. M., C. D. Charles, H. Cheng, and R. L. Edwards (2003), El Niño-Southern Oscillation and tropical Pacific climate during the last millenium, *Nature*, *424*, 271–276.

Collins, M. (2000), Understanding Uncertainties in the response of ENSO to greenhouse warming, *Geophys. Res. Lett.*, *27*, 3509–3513.

Corrège, T., T. Delcroix, J. Récy, W. Beck, G. Cabioch, and F. Le Cornec (2000), Evidence for stronger El Niño-Southern Oscillation (ENSO) events in a mid-Holocene massive coral, *Paleoceanography*, *15*, 465–470.

Fedorov, A. V., and S. G. H. Philander (2000), Is El Niño changing?, *Science*, *288*, 1997–2002.

Gill, A. E. (1982), *Atmosphere-Ocean Dynamics*, Academic, San Diego, Calif.

Goosse, H., F. M. Selten, R. J. Haarsma, and J. D. Opsteegh (2002), Large sea-ice volume anomalies simulated in a coupled climate model, *Climate Dyn.*, *10*, doi:10.1007/s0,382-002-0290-4.

Hewitt, C. D., A. J. Broccoli, J. F. B. Mitchell, and R. J. Stouffer (2001), A coupled model of the last glacial maximum: Was part of the North Atlantic relatively warm?, *Geophys. Res. Lett.*, *28*, 1571–1574.

Hughen, K. A., D. P. Schrag, and S. B. Jacobsen (1999), El Niño during the last interglacial period recorded by a fossil coral from Indonesia, *Geophys. Res. Lett.*, *26*, 3129–3132.

Jin, F. (1997), An equatorial ocean recharge paradigm for ENSO, part I: Conceptual model, *J. Atmos. Sci.*, *54*, 811–829.

Jin, F., S. An, A. Timmermann, and J. Zhao (2003), Strong El Niño events and nonlinear dynamical heating, *Geophys. Res. Lett.*, *30*(3), 1120, doi:10.1029/2002GL016356.

Kang, I.-S., S.-I. An, and F.-F. Jin (2001), A systematic approximation of the sst anomaly equation for ENSO, *J. Meteorol. Soc. Jpn.*, *79*, 1–10.

Kim, S. J., G. M. Flato, and G. J. Boer (2003), A coupled climate model simulation of the last glacial maximum, part 2: Approach to equilibrium, *Clim. Dyn.*, *20*, 635–661.

Kitoh, A., S. Muakami, and H. Koide (2001), A simulation of the Last Glacial Maximum with a coupled atmosphere-ocean AGCM, *Geophys. Res. Lett.*, *28*, 2221–2224.

Koutavas, A., J. Lynch-Stieglitz Jr., T. M. Marchitto, and J. P. Sachs (2002), El Niño-like pattern in ice age tropical Pacific sea surface temperature, *Science*, *297*, 226–230.

Lea, D. W., D. K. Pak, and H. J. Spero (2000), Climate impact of late Quaternary equatorial Pacific sea surface temperature variations, *Science*, *289*, 1719–1724.

Liu, Z. (2002), A simple model study of ENSO suppression by external periodic forcing, *J. Clim.*, *15*, 3518–3522.

Liu, Z., S. Shin, B. Otto-Bliesner, J. E. Kutzbach, E. C. Brady, and D. Lee (2002), Tropical cooling at the Last Glacial Maximum and extratropical ocean ventilation, *Geophys. Res. Lett.*, *29*(10), 1409, doi:10.1029/2001GL013938.

Moy, C. M., G. O. Seltzer, D. T. Rodbell, and D. M. Anderson (2002), Variability of El Niño/Southern Oscillation activity at millenial timescales during the Holocene epoch, *Nature*, *420*, 162–165.

Otto-Bliesner, B. L., E. C. Brady, S. Shin, Z. Liu, and C. Shields (2003), Modeling El Niño and its tropical teleconnections during the last glacial-interglacial cycle, *Geophys. Res. Lett.*, *30*(23), 2198, doi:10.1029/2003GL018553.

Peltier, W. R., and L. P. Solheim (2004), The climate of the Earth at Last Glacial Maximum: Statistical equilibrium state a mode of internal variability, *Quat. Sci. Rev.*, *23*, 335–357.

Rittenour, T. M., J. Brighan-Grette, and M. E. Mann (2000), El Niño-Like climate teleconnection in New England during the late Pleistocene, *Science*, *288*, 1039–1042.

Rodbell, D. T., G. O. Seltzer, D. M. Anderson, M. B. Abbott, D. B. Enfield, and J. H. Newman (1999), An 15000-year record of El Niño-driven alluviation in southwestern Ecuador, *Science*, *283*, 516–519.

Sandweiss, D. H., J. B. Richardson, E. J. Reitz, H. B. Rollins, and K. A. Maasch (1996), Geoarcheological evidence from Peru for a 5000 years B.P. onset of El Niño, *Science*, *273*, 1531–1533.

Shin, S. I., Z. Liu, B. L. Otto Bliesner, E. C. Braday, J. E. Kutzbach, and S. P. Harrison (2003), A simulation of the Last Glacial Maximum Climate using the NCAR CSM, *Clim. Dyn.*, *20*, 127–151.

Timmermann, A. (2001), Changes of ENSO stability due to greenhouse warming, *Geophys. Res. Lett.*, *28*, 2064–2068.

Timmermann, A., M. Latif, A. Bacher, J. M. Oberhuber, and E. Roeckner (1999), Increased El Niño frequency in a climate model forced by future greenhouse warming, *Nature*, *398*, 694–696.

Timmermann, A., F. Justino, H. Goosse, and F.-F. Jin (2004), Surface temperature control in the North and tropical Pacific during the last glacial period, *Clim. Dyn.*, *23*, 353–370.

Trefethen, L. N. (1999), Computation of pseudospectra, *Acta Numer*, 8, 247–295.

Tudhope, A. W., C. P. Chilcott, M. T. McCulloch, E. R. Cook, J. Chappell, R. M. Ellam, D. W. Lea, J. M. Lough, and G. B. Shimmield (2001), Variability in the El Niño-Southern Oscillation through a glacial-interglacial cycle, *Science*, 291, 1511–1517.

Woodroffe, C. D., M. R. Beech, and M. K. Gagan (2003), Mid-late Holocene El Niño variability in the equatorial Pacific from coral microatolls, *Geophys. Res. Lett.*, 30(7), 1358, doi:10.1029/2002GL015868.

Zebiak, S. E., and M. A. Cane (1987), A model El Niño-Southern Oscillation, *Mon. Weather Rev.*, 115, 2262–2278.

———————————

S.-I. An, International Pacific Research Center, University of Hawaii, 2525 Correa Road, Honolulu, HI 96822, USA.

L. Bejarano and F.-F. Jin, Department of Meteorology, Florida State University, 404 Love Building, Tallahassee, FL 32306-4520, USA.

F. Justino, Department of Physics, University of Toronto, 60 St. George Street, Toronto, Ontario, Canada M5S 1A7.

Z. Liu, Center for Climatic Research, University of Wisconsin-Madison, 1225 West Dayton Street, Madison, WI 53706, USA.

A. Timmermann (corresponding author), International Pacific Research Center, University of Hawaii, 2525 Correa Road, Honolulu, HI 96822, USA. (axel@hawaii.edu)

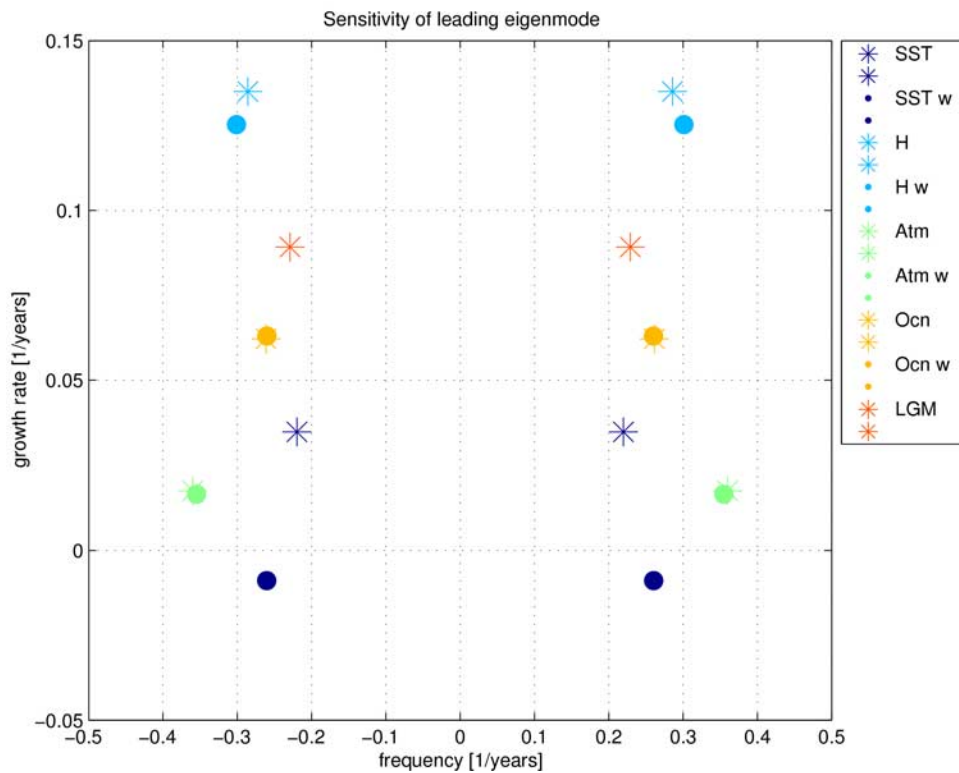A. W. Tudhope, School of Geosciences, Edinburgh University, West Mains Road, Edinburgh, EH9 3JW, UK.
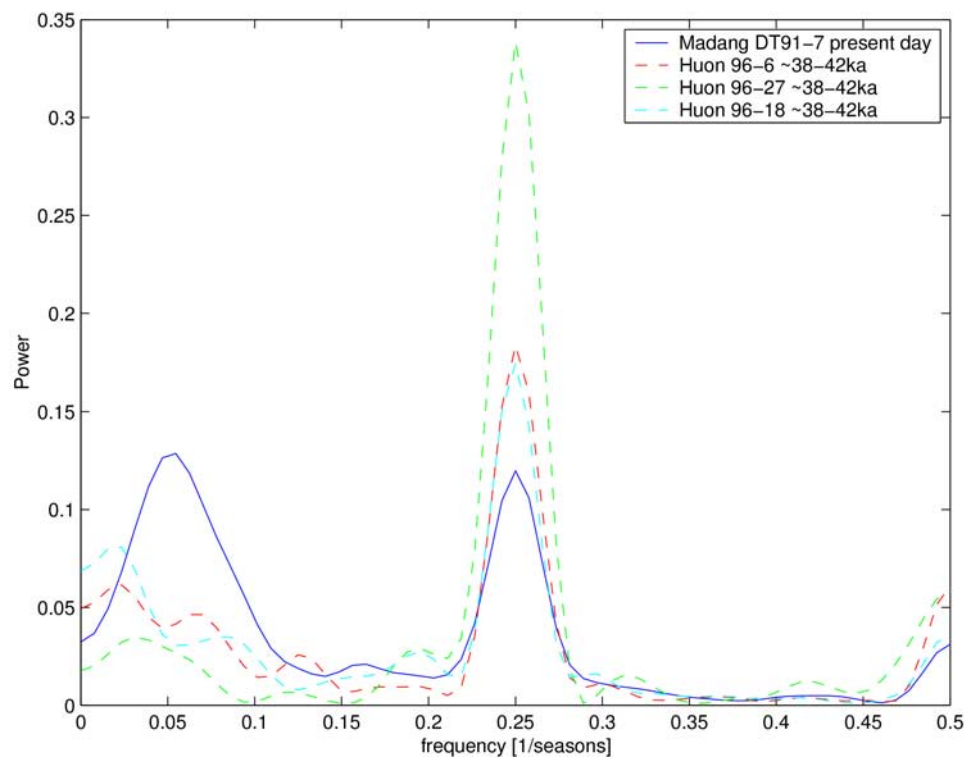
Figure 1. Power spectra of $\delta^{18}O$ time series obtained from an isotope analysis of fossil (dashed) and modern (solid) corals sampled in Papua New Guinea. Data from *Tudhope et al.* [2001].
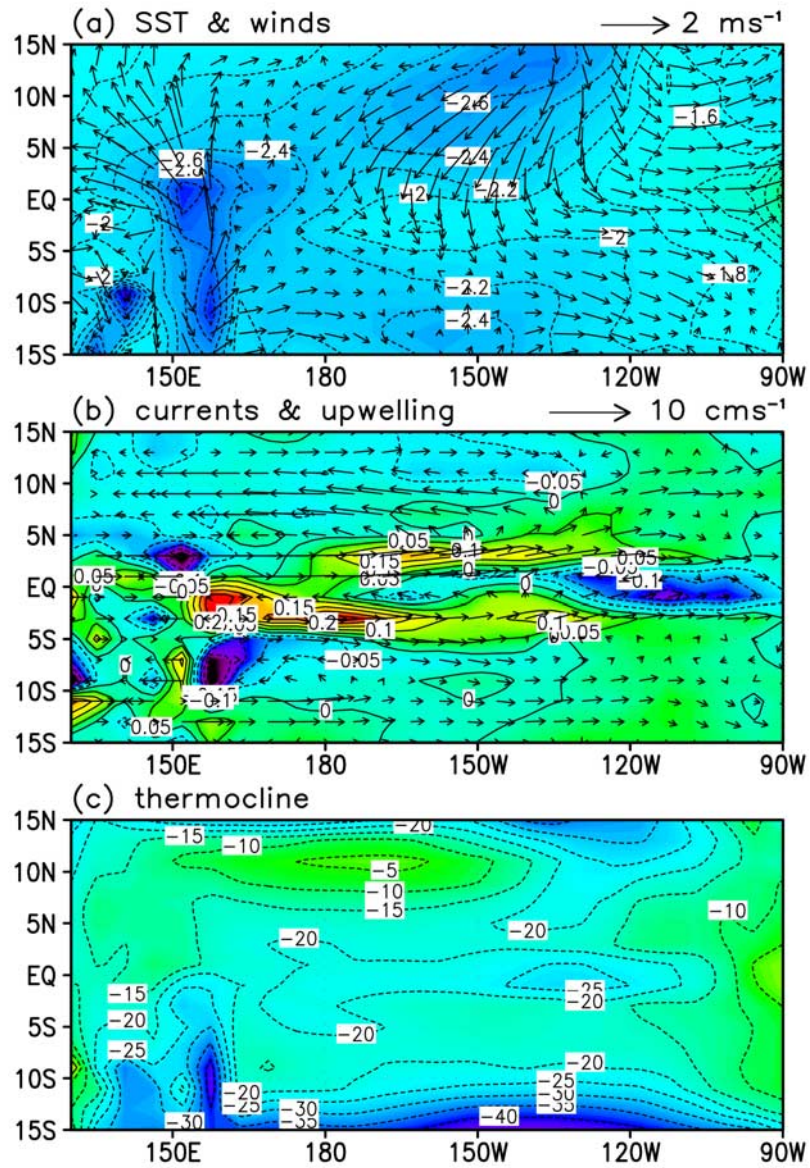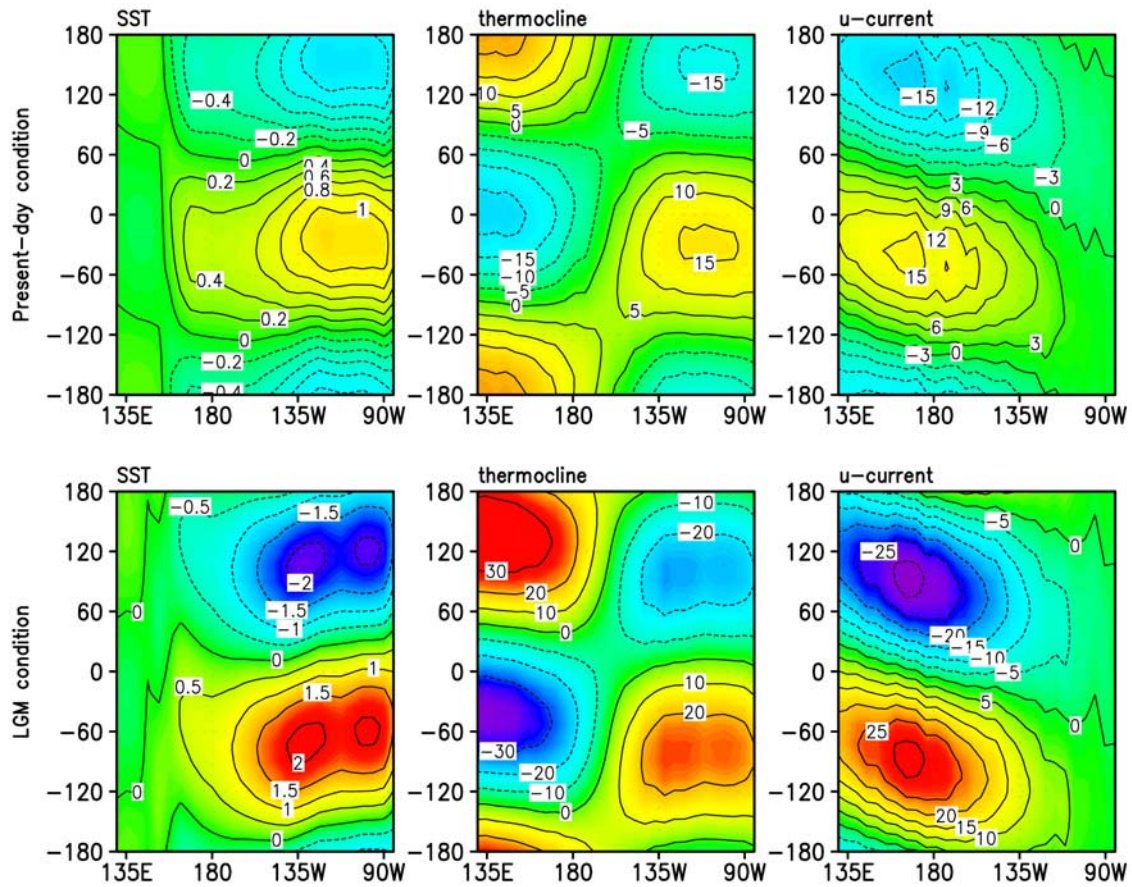
Figure 2. Simulated difference of SST (K), wind (m/s), surface current (cm/s), upwelling (10^{-3}cm/s) and thermocline depth (m) between CSM LGM and present-day simulation. Data are interpolated onto the grid of our intermediate tropical model.
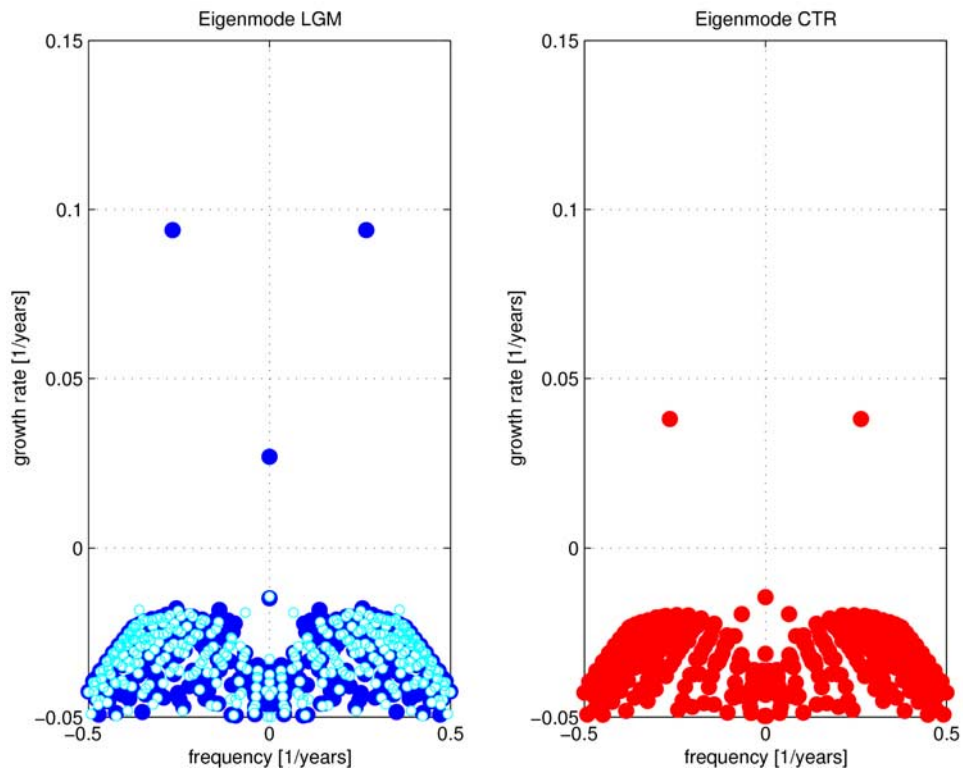
Figure 3. Eigenmodes of the linearized ZC-type intermediate ENSO model for (left) glacial and (right) present-day background conditions as simulated by the CSM1.4 model. The light blue dots represent the leading eigenmode using LGM background conditions if extratropical anomalies are neglected. The eigenspectrum is symmetric around the zero frequency.

Figure 4. Sensitivity of the leading eigenmodes of the linearized ZC-type intermediate ENSO model with respect to latitudinal weighting (w) and LGM changes in only one variable of the climate background conditions. SST indicates LGM changes are taken into account only for the SST background field. Abbreviations are as follows: H, thermocline depth changes; Atm., wind and wind-divergence changes; Ocn., changes of the oceanic currents; LGM, changes of all background fields.
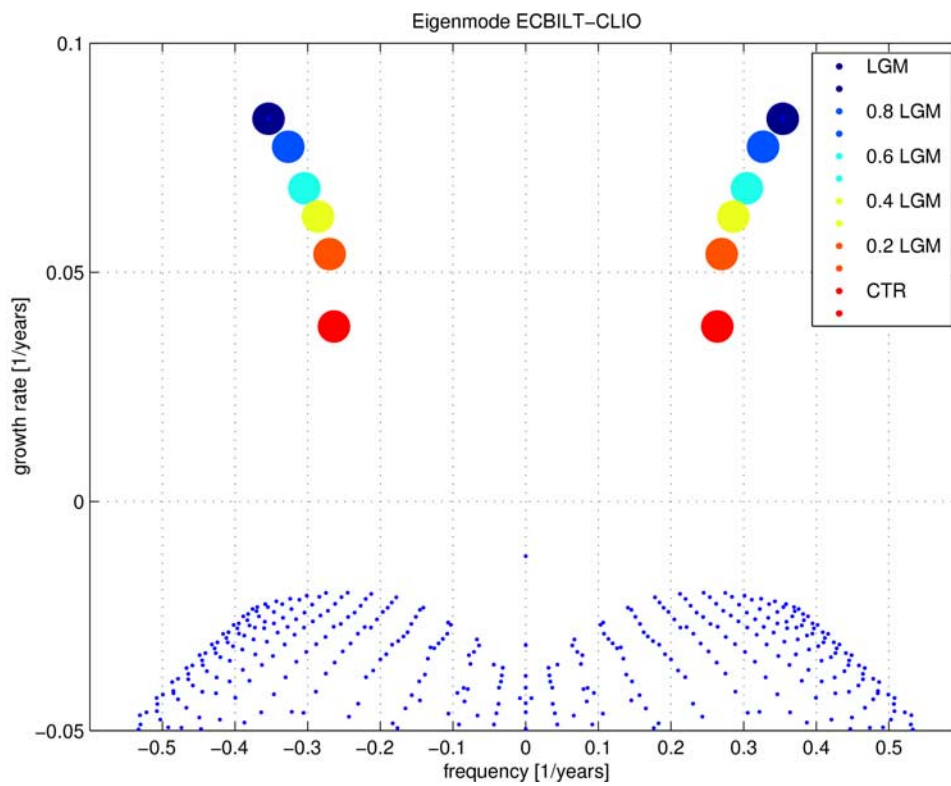
Figure 5. Hovmoller diagram of the leading eigenvector of the linearized ZC-type intermediate ENSO model for observed (upper panels) present-day and (lower panels) glacial background conditions simulated by the CSM model. Only the SST, thermocline depth, and current anomalies are displayed. The time evolution represented by the phase on the y axes is directed upward.
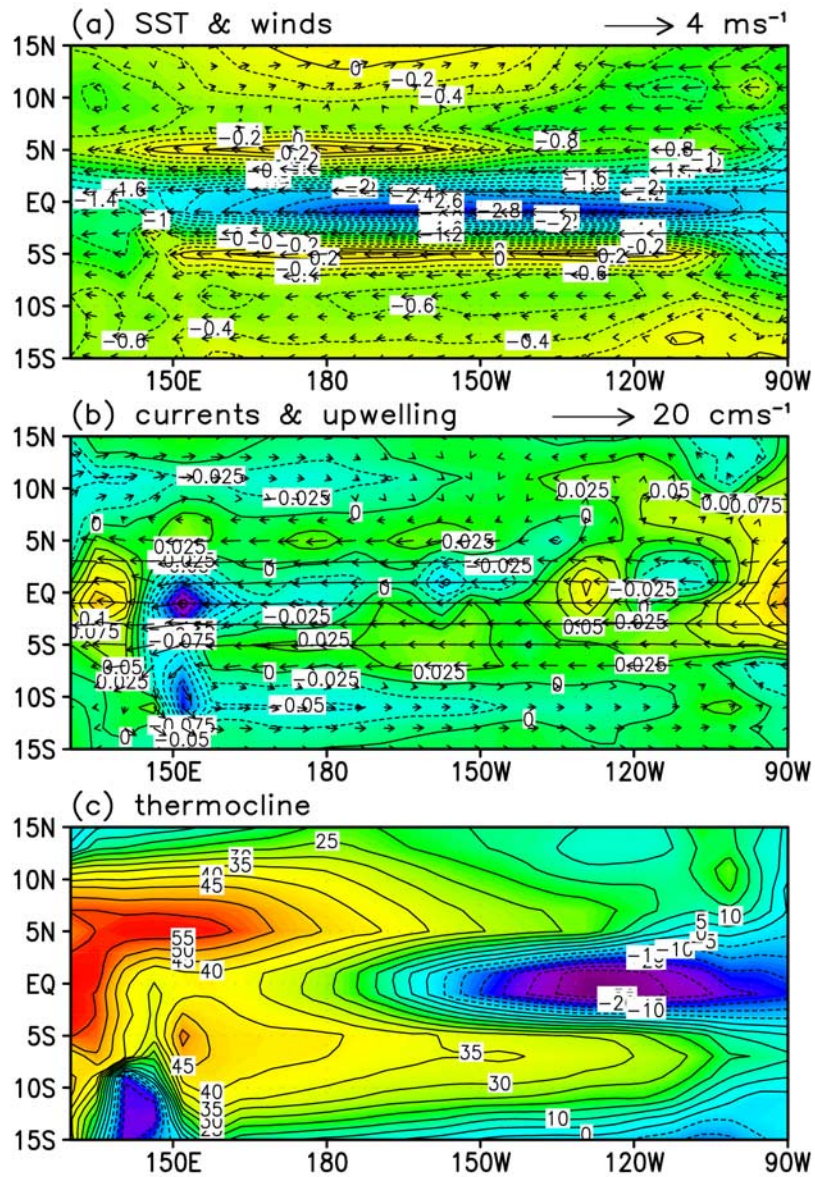
Figure 6. Simulated difference of SST (K), wind (m/s), surface current (cm/s), upwelling (10^{-3}cm/s) and thermocline depth (m) between ECBilt-CLIO LGM and present-day simulation. Data are interpolated onto the grid of our intermediate tropical model.

Figure 7. Eigenmode spectrum (dark blue) for the LGM background perturbation simulated by the ECBilt-CLIO model. Colored dots: Leading eigenmodes for different values of γ as defined by $\vec{X}_{BG} = \vec{X}_{ZC} + \gamma(\vec{X}_{LGM} - \vec{X}_{CTR})$. Red dot: leading eigenmode of the intermediate ENSO model forced by present-day climate background conditions.